CONF-900403--3

STRESS CORROSION CRACKING OF CANDIDATE MATERIALS FOR NUCLEAR WASTE CONTAINERS*

by

CONF-900403--3

DE90 003827

P. S. Maiya, W. J. Shack, and T. F. Kassner

Materials and Components Technology Division
Argonne National Laboratory
Argonne, Illinois 60439 USA

September 1989

Submitted for presentation at CORROSION/90, Las Vegas, NV, April 23-27, 1990 T2A Symposium-Corrosion of Materials in Nuclear Systems.

*Work performed for the U. S. Department of Energy under subcontract from Lawrence Livermore National Laboratory (ACK 85861).

STRESS CORROSION CRACKING OF CANDIDATE MATERIALS FOR NUCLEAR WASTE CONTAINERS*

by

P. S. Maiya, W. J. Shack, and T. F. Kassner
Materials and Components Technology Division
Argonne National Laboratory
Argonne, IL 60439

ABSTRACT

Types 304L and 316L stainless steel (SS), Incoloy 825, Cu, Cu-30%Ni, and Cu-7%Al have been selected as candidate materials for the containment of high-level nuclear waste at the proposed Yucca Mountain Site in Nevada. The susceptibility of these materials to stress corrosion cracking has been investigated by slow-strain-rate tests (SSRTs) in water which simulates that from well J-13 (J-13 water) and is representative of the groundwater present at the Yucca Mountain site. The SSRTs were performed on specimens exposed to simulated J-13 water at 93°C and at a strain rate 10^{-7} s^{-1} under crevice conditions and at a strain rate of 10^{-8} s^{-1} under both crevice and noncrevice conditions. All the tests were interrupted after nominal elongation strains of 1-4%. Examination by scanning electron microscopy showed some crack initiation in virtually all specimens. Optical microscopy of metallographically prepared transverse sections of Type 304L SS suggests that the crack depths are small (<10 μm). Preliminary results suggest that a lower strain rate increases the severity of cracking of Types 304L and 316L SS, Incoloy 825, and Cu but has virtually no effect on Cu-30%Ni and Cu-7%Al. Differences in susceptibility to cracking were evaluated in terms of a stress ratio, which is defined as the ratio of the increase in stress after local yielding in the environment to the corresponding stress increase in an identical test in air, both computed at the same strain. On the basis of this stress ratio, the ranking of materials in order of increasing resistance to cracking is: Types 304L SS< 316L SS<Incoloy 825 ≅ Cu-30%Ni<Cu ≅ Cu-7%Al.

---

*Work supported by the U. S. Department of Energy under subcontract from Lawrence Livermore National Laboratory.

INTRODUCTION

The Yucca Mountain Project is investigating the feasibility of locating a repository for high-level nuclear waste in tuff formations in southern Nevada. The nuclear waste, in waste containers, must be isolated from the environment for at least 300 to 1000 years after emplacement. Currently, six candidate materials for the waste containers are being considered at Lawrence Livermore National Laboratory (LLNL),[1] namely, Types 304L and 316L stainless steel (SS), Incoloy 825, phosphorus-deoxidized copper (Cu), Cu-30%Ni, and Cu-7%Al. These materials were chosen because of their favorable corrosion properties and their extensive use in marine, nuclear, and process industries.[2]

Although relatively little water is expected to reach the containers, and for much of the time the temperatures will be sufficiently high that any water in the vicinity of the waste containers will be present only in the form of steam, the present study focuses on aqueous environments at ~93°C, since these environments are expected to provide the "worst case" conditions for susceptibility to stress corrosion cracking (SCC). The elemental composition of water from well J-13 (J-13 water),[3], which is representative of the groundwater present at the Yucca Mountain Site, is summarized in Table 1.

This paper provides some slow-strain-rate test (SSRT) results and methods of analysis used to rank the materials in terms of their resistance to SCC.

EXPERIMENTAL DETAILS

Materials

Cylindrical SSRT specimens (with a 6.35-mm diameter by 36.0-mm gauge length) were fabricated from 25.4-mm-thick annealed plates of Types 304L and 316L SS, Incoloy 825, Cu (CDA-122), Cu-30%Ni (CDA-715), and Cu-7%Al (CDA-614) supplied by LLNL. The chemical analyses and heat numbers are given in Tables 2 and 3. As shown in Fig. 1, two small-diameter (~0.8-0.9 mm) through holes in the gauge section of the specimen

localize the strain and cracking and thereby facilitate observation of SCC by scanning electron microscopy (SEM). When pins of matching materials are inserted in the holes, crevices are produced. Similar specimens were used in our earlier studies on SCC of austenitic stainless steels in simulated boiling water reactor environments.[4,5]

Techniques and Procedures

The SSRTs were conducted in simulated J-13 water at 93°C and at strain rates of 10^{-7} and 10^{-8} s^{-1}. The tests were interrupted after elongation (plastic) strains of 1-4% were reached. A worm gear Jactuator, gear reducers, and a variable-speed control system were used to apply the strain. The temperature was maintained by clamp-on heaters with associated instrumentation. A once-through water system with a flow rate of ~3 mL/min was used. The tests were conducted in a 1.27-L nickel container.

A schematic representation of the SSRT system, including the feedwater system and the electrochemical-potential (ECP) monitoring system, is shown in Fig. 2. A dial indicator was used to measure the displacement of the pull rod. This measurement, along with measurements of the system compliance, can be used to estimate the extension of the specimen during the test. Measurements of total specimen length before and after the tests give values of the actual elongation (plastic strain) that are even more accurate . After each test, the specimen was sectioned by electrical discharge machining (EDM), as shown in Fig. 3, so that the entire hole region could be examined by SEM at magnifications up to 2000X to detect stress corrosion cracks.[5]

In the tests on materials at a strain rate of 10^{-7} s^{-1}, pins of a matching material were inserted into the two holes to produce crevices. The tests were interrupted after elongations of 3-3.7%. During the tests, siphon action in the inverted drain tube shown in Fig. 2 exposes the top crevice alternately to water in the liquid and vapor phases whereas the bottom crevice is always kept immersed in liquid. Both crevices can be exposed to the liquid phase only by opening the hole at the top of the drain tube to the

atmosphere.

Tests were also performed at a strain rate of 10^{-8} s^{-1} to investigate the effect of strain rate on SCC. In these tests, one of the holes was left open, but a pin was inserted in the other hole to produce a crevice. The entire specimen was continuously exposed to water. These changes were made to determine whether a crevice is necessary for cracking of the materials. These tests were interrupted after plastic elongation strains of ~1.0–1.6%, which are somewhat lower than the strains at which the tests at the higher strain rate were interrupted.

Monitoring of Water Chemistry and Electro-chemical Potential

For the tests conducted at a strain rate of 10^{-7} s^{-1}, the water chemistry approximated that of J-13 water (see Table 1); however, the concentrations of some of the anions (F^-, Cl^-, and NO_3^-) were higher by factors of ~2–20 and concentration of HCO_3^- was lower by factors of ~2–4. The required 30 ppm Si (~80 ppm SiO_3^{2-}) and 19–78 ppm HCO_3^-) in the feedwater were obtained by the addition of Na_2SiO_3 and by sparging the feedwater with a 12% CO_2–20% O_2–68% N_2 gas mixture. This gas mixture set the dissolved oxygen concentration of the feedwater at ~7–8 ppm. An overpressure of 5 psig was maintained in the feedwater tank, and the $pH_{25°C}$ of the effluent water ranged from 6.9 and 7.8. Nickel from corrosion of the test vessels was detected in the effluent water, typically in a concentration of <2 ppm.

For the tests conducted at a strain rate of 10^{-8} s^{-1}, the concentration of the HCO_3^- species was increased to the level in well J-13 water (i.e, to ~143 ppm) by adding $NaHCO_3$, sparging the feedwater with the 12% O_2–20% O_2–68%N_2 gas mixture and maintaining a 5 psig overpressure. This procedure, which stabilized the HCO_3^- concentration and pH of the feedwater, resulted in achieving the desired dissolved oxygen concentration. The HCO_3^- and $pH_{25°C}$ values in the effluent water range varied between 125 and 141 ppm and 7.8 and 8.5, respectively. Na_2SiO_3 was no longer added to the feedwater to prevent precipitation of SiO_2, $CaSiO_3$, and $MgSiO_3$. With the exception of the Si concentration (<0.1 ppm), this water chemistry is a

good simulation of the ionic and dissolved-gaseous species in J-13 water, although the $pH_{25°C}$ values are still somewhat higher than the reported near-neutral value for J-13 water. This, in part, can be attributed to some loss of CO_2 to the gas phase at ambient pressure above the water (i.e., air trapped by a snug metal lid that fits on top of the test vessel).

ECP of the insulated SSRT specimens was measured at regular intervals against an external 2×10^{-4} M KCl/AgCl/Ag reference electrode during the test to determine the steady-state potential. To minimize changes in electrolyte concentration, the concentration of the KCl in the electrolyte was approximately the same as the concentration of K^+ and Cl^- ions in the test environments. An example of the measured ECP of the Cu-7%Al alloy specimen versus time in test W15 is shown in Fig. 4. The measured ECP values were also converted to the standard hydrogen electrode (SHE) scale.[6] An experimental SHE correction potential of +378 mV was obtained for this electrlyte versus a commonly used 0.1 M KCl/Ag/AgCl reference electrode and this value was used to convert the steady-state ECP values to the SHE scale. The calculated value for the electrolyte concentration of 2×10^{-4} M is +365 mV.

RESULTS AND DISCUSSIONS

SEM Observations

The SSRT parameters are summarized in Tables 4 and 5. The SEM observations for all the tests conducted at a strain rate of 10^{-7} s^{-1} are summarized in Table 6, which showed that some cracking was observed in virtually all the specimens. Cracking was also observed in specimens tested at a slower strain rate of 10^{-8} s^{-1}. However, in most cases, crack observations were made at magnifications as high as 1000-2000X, since it was difficult to observe well-defined cracks at magnifications lower than 100X. Hence the actual crack depths, which can be inferred from the size of the crack opening are small (in the micron range) even for Type 304L SS. The cracks in Type 304L SS are more open (and hence are probably deeper) than those in Incoloy 825, as shown in Fig. 6. This is consistent with the expected greater resistance of Incoloy 825 to SCC because of its higher

nickel content.[7] However, Incoloy 825 shows a larger number of cracks than Type 304 SS.

The inference from the SEM observations, that the cracks are shallow, is consistent with our unsuccessful efforts, thus far, to observe cracks >10–20 μm in depth in transverse metallographic specimens of Type 304L SS. Multiple sections were examined by successively grinding away ~0.1–0.13 mm of material and metallographically preparing the resulting new surface. Even after as much as ~0.5 mm of material had been removed in this manner, only small cracks (~10 μm in depth) were observed. Such cracks have not been observed in unstressed but geometrically similar specimens exposed to simulated J–13 water at 93°C for the same length of time as that elapsed for stressed Type 304L SS (Test W4).

Scanning electron microscopy of the Cu and Cu–base alloy specimens showed that these materials also crack in simulated J–13 water. There were no discernible differences in cracking among the three Cu–base materials.. It appears that the differences in susceptibility to SCC of these three materials are small compared to the differences, for example, between Type 304L SS and Incoloy 825. Further quantification of SCC in terms of crack depths and crack growth rates is required to better delineate differences in cracking behavior.

The cracking in crevices that were continuously exposed to liquid phase was not much different from that for crevices alternately exposed to liquid and vapor phases. This is illustrated in Fig. 6 for an Incoloy 825 specimen. In tests conducted at a strain rate of 10^{-8} s^{-1}, cracking at the holes with pins (crevice) and those without pins (noncrevice) is similar for all the materials examined thus far. Hence, it appears that a crevice is not required for SCC in these materials under these conditions.

On the basis of the SEM observations, it is difficult to determine whether the change in strain rate had any effect on cracking, since the observed differences are small, and furthermore, the tests performed at the slower strain rate of 10^{-8} s^{-1} were interrupted at lower strains than those performed at a strain rate of 10^{-7} s^{-1} (see Tables 4 and 5). There were also small variations in water chemistry in the tests conducted at the two strain

rates, as discussed earlier. But the two SSRTs conducted on Incoloy 825 at a strain rate of 10^{-7} s^{-1} in different environments, one in simulated J-13 water, and the other in the presence of ~20 times greater ionic concentration of impurities, showed no difference in cracking, as determined by SEM after approximately the same elongation strains. Therefore, changes in impurity concentration in the tests are not expected to influence cracking in a significant manner. As will be discussed later, the stress-deformation histories during the SSRTs suggest that, at least for some materials such as Incoloy 825, SCC was more significant at the lower strain rate but was not affected by changes in the simulated J-13 water chemistry.

Estimation of Local Plastic Strains

To relate the observed crack initiation and growth to plastic strain, it is necessary to estimate the local plastic strain at the hole. The local strain is computed as the product of a strain concentration factor K_ε, estimated from Neuber's rule, and the nominal strain in the unreduced gauge section, which is determined from the stress-strain curve and the measured load on the specimen.

Stress-strain data for these materials can be described by the frequently used Ramberg and Osgood equation[8]

$$\varepsilon = \frac{\sigma}{E} + \alpha\left(\frac{\sigma}{E}\right)^m \qquad (1)$$

where σ and ε are the nominal stress and strain, respectively, E is the Young's modulus, and α and m are constants. Locally, near the hole, the stress and strain are then given by

$$K_\varepsilon\,\varepsilon = \frac{\sigma K_\sigma}{E} + \alpha\left(\frac{\sigma K_\sigma}{E}\right)^m \qquad (2)$$

where K_ε and K_σ are the strain and stress concentration factors, respectively. Substitution of Neuber's rule[9]

$$K_\varepsilon = \frac{K^2}{K_\sigma} \qquad (3)$$

(where K is the theoretical elastic stress concentration factor) in Eq. (2) gives

$$\frac{K^2}{K_\sigma} = \frac{\varepsilon_e K_\sigma}{\varepsilon_e + \varepsilon_p} + K_\sigma^m \alpha \frac{\varepsilon_e^m}{\varepsilon_e+\varepsilon_p}. \tag{4}$$

Rewriting Eq. (1) in the following form

$$\varepsilon_p = \alpha \varepsilon_e^m \tag{5}$$

(where $\varepsilon_p = \varepsilon - \sigma/E$) and substituting Eq. (5) in Eq. (4) yields

$$K^2 = K_\sigma^2 \left(\frac{\varepsilon_e}{\varepsilon_e + \varepsilon_p}\right) + K_\sigma^{m+1} \left(\frac{\varepsilon_p}{\varepsilon_e + \varepsilon_p}\right). \tag{6}$$

Equation (6) can also be expressed as

$$K^2 = K_\sigma^2 \left(\frac{\beta}{1+\beta}\right) + K_\sigma^{n+1} \left(\frac{1}{1+\beta}\right) \tag{7}$$

where $\beta = \frac{\varepsilon_\varepsilon}{\varepsilon_p}$ Since K is known (for the SSRT specimen containing a through hole K ≈ 3), Eq. (7) can be solved with smooth specimen stress–strain data to estimate the actual stress concentration factor K_σ at the hole. The actual strain concentration can then be determined by applying Neuber's rule [Eq. (3)].

Stress-strain curves were determined for all the materials from conventional tensile tests in air at a strain rate of ~4.7×10^{-4} s^{-1}. These stress–strain data were analyzed by use of the Ramberg and Osgood equation and Neuber's rule to determine the strain concentration at the hole as function of plastic strain. As an example, the results for Cu in Fig. 7 show that the strain concentration factor decreases with plastic strain as expected.

The strain concentration, K_ε, can also be computed by using a simple

power-law relation between stress and plastic strain, i.e.,

$$\sigma = \frac{E}{\alpha^n}\,\varepsilon_p^n = \sigma_o\,\varepsilon_p^n \tag{8}$$

where $n = \frac{1}{m}$ and $\sigma_o = \frac{E}{\alpha^n}$. Locally, near the hole,

$$K_\sigma\,\sigma = \sigma_o\,(K_\varepsilon \varepsilon_p)^n. \tag{9}$$

Equations (8) and (9) imply that

$$K_\sigma = K_\varepsilon^n. \tag{10}$$

Substituting Eq. (10) in Neuber's rule, Eq. (3), gives

$$K^2 = K_\varepsilon^{n+1} \tag{11}$$

and solving for K_ε

$$K_\varepsilon = K^{\frac{2}{1+n}}. \tag{12}$$

The two approaches for estimating K_ε give almost identical results even for relatively low plastic strains, as shown in Fig. 7.

The local strains in Tables 4 and 5 are computed under the assumption that the stress-strain data generated at a strain rate of ~2.2 x 10^{-4} s^{-1} at room temperature can be applied to the SSRT results at a much slower strain rate and at a slightly higher temperature. The nominal strain in the unreduced section is determined from the stress-strain curve corresponding to the load at which the SSRTs tests were interrupted. The strain concentration factor is determined from Eq. (12) with a value of n appropriate for the strain in the tests. The local plastic strains varied between 8 and15% for the tests at a strain rate of 10^{-7} s^{-1} (Table 4) and are lower (2.3–4.5%) for tests conducted at a strain rate of 10^{-8} s^{-1} (Table 5).

Relative SCC Susceptibility of Waste Container Materials

To obtain additional information on the relative cracking susceptibility of the various materials, the load-deformation behavior of specimens during the SSRTs was analyzed, and a cracking index parameter or stress ratio (SR) was formulated based on comparing the stress in the environment with that in air at the same plastic strain. For the present geometry, the SR, which characterizes the effect of the environment on the capability of material to sustain load in the plastic range, can be defined as

$$SR = \left(\frac{\sigma_{en} - \sigma_y/3}{\sigma_{air} - \sigma_y/3}\right)_{\epsilon_p} \qquad (13)$$

where σ_{en} is the nominal stress in the environment, σ_{air} is the nominal stress in air, evaluated at the same plastic strain, and σ_y is the yield stress of the material. To minimize geometry effects, σ_{en} and σ_{air} are determined for the same specimen geometry. Local plastic yielding is assumed to occur when the nominal stress reaches $\sigma_y/3$, since the stress concentration factor for the present specimen geometry is ~3. The use of stress instead of load eliminates any possible differences resulting from variations in specimen diameter. The ratio focuses on the changes in stress after plastic yielding occurs, since SCC is not expected without plastic deformation. By eliminating the elastic contribution to the stress, the cracking index, or SR, appears to provide a sensitive indicator of SCC and is useful for screening materials, at least on a qualitative basis. As currently computed, we assume that the differences in strain rate between the in-air tests and the SSRTs do not significantly affect the stress-strain response at the temperature of interest. With no cracking the SR is = 1; if the material is susceptible to cracking, the value is < 1. However, a measured value of 1 may only indicate that the degree of cracking is so small that the change in loads cannot be detected. Although values of SR <1 indicate that cracking has occurred, tests at various strain rates are needed to determine whether the cracking is environmentally assisted or not.

To determine the stress ratio, the strains in the SSRT must be known. By measuring the pull-rod displacement during a test, strains can be

determined in "real time" by determining the compliance of the SSRT machine and then using the measured compliance to compute the strain from the measured loads and displacements, as is done in a conventional tensile test. Somewhat more accurate estimates can be obtained post-test from the measured final plastic strain and load at the time of interruption of the tests. The total strain at the end of the test ε_{final} is then

$$\varepsilon_{final} = \varepsilon_{p\ final} + \frac{\sigma_{final}}{E} \tag{14}$$

where the stress is computed from the final load and the initial crosssection of the specimen. The total and plastic strains as a function of time, $\varepsilon(t)$ and $\varepsilon_p(t)$, respectively, of the specimen are computed by the following equations assuming a constant strain rate $\dot{\varepsilon}$:

$$\varepsilon(t) = \varepsilon_{final} - \dot{\varepsilon}\,[t_{final} - t]. \tag{15}$$

$$\varepsilon_p(t) = \varepsilon(t) - \frac{\sigma(t)}{E}. \tag{16}$$

Calibration tests show the assumption of a constant strain rate to be quite good, once yielding has occurred. Thus, plastic strains greater than ~0.5% may by accurately determined. The yield stress σ_y for all the six materials required for the computation of the stress ratio is listed in Table 7.

Figure 8 shows the variation of SR with plastic strain at a strain rate of 10^{-7} s^{-1} for the six materials in simulated J-13 water at 93°C. The ranking of materials in order of increasing resistance to cracking is as follows: Type 304L SS<Type 316L SS<Incoloy 825 ≅ Cu-30%Ni<Cu ≅ Cu-7%Al. Phosphorus-deoxidized Cu and Cu-7%Al (aluminum bronze) appear to be more resistant to cracking than the other alloys. The higher cracking resistance of Incoloy 825 compared to Type 304L SS can be attributed to the higher nickel content of Incoloy 825, and is qualitatively consistent with SEM observations of the cracks. The differences in the cracking behavior of Incoloy 825, Cu-30%Ni, Cu, and Cu-7%Al are small, which is also qualitatively consistent with the SEM observations. Somewhat surprisingly,

the SR appears to be fairly sensitive to cracking, even when the cracks are too small to be readily observed metallographically.

A strain ratio analogous to the SR can be defined as follows:

$$\text{Strain ratio} = \left(\frac{\varepsilon_{p(air)}}{\varepsilon_{p(en)}}\right)_{\sigma} \qquad (17)$$

where the strain in air and in the environment are evaluated at the same nominal stress. As can be seen from Fig. 9, the SCC susceptibility rankings determined from the two ratios are similar. However, the strain ratio indicates a greater degree of susceptibility of Type 304L SS relative to Type 316L SS than is suggested by the stress ratio. Values of the strain ratio at the end of the tests are included in Tables 4 and 5.

Influence of Strain Rate on SCC

Whereas the strain rate appears to influence the SR of Type 304L SS and Incoloy 825, as shown in Figs. 10 and 11, respectively, it has no effect on Cu–30%Ni, as shown in Fig. 12. The strain rate also appears to influence the SR of Type 316L SS and Cu, but it has virtually no effect on Cu–7%Al. In the cases where a strain-rate effect on SR was observed, lowering the strain rate decreased the value of SR. The absence of a strain-rate effect suggests that if a decrease in the value of SR is associated with an increase in cracking (as is expected on the basis of our formulation), our preliminary results suggest that the cracking observed for the Cu–30%Ni and Cu–7%Al alloys may not be SCC. Further work is in progress to better understand the relationship between SR and susceptibility to cracking in SSRTs and also to confirm the preliminary findings on the relative SCC susceptibility of these materials by fracture-mechanics tests.

SUMMARY AND CONCLUSIONS

A series of slow strain rate tests (SSRTs) on six candidate materials for nuclear waste containers was conducted under both crevice and noncrevice conditions in simulated J–13 water at 93°C, at strain rates of 10^{-7} and

10^{-8} s^{-1}. All the tests were performed under approximately identical conditions of electrochemical potential. The specimens contained small-diameter through holes (with or without pins of the matching material) to facilitate observation of cracks by scanning electron microscopy, which showed cracking in virtually all the materials under the severe testing conditions employed. Susceptibility to cracking was evaluated on the basis of a stress ratio (SR), which is defined as the ratio of the increase in stress following the initiation of local yielding for the material in the environment to the corresponding stress increase for an identical test in air at the same elongation. On the basis of this SR, the ranking of the materials in order of increasing resistance to cracking is: Type 304L SS<Type 316L SS<Incoloy 825 ≡ Cu–30%Ni<Cu ≡ Cu–7%Al. The cracking index suggests that a lower strain rate has a deleterious effect on cracking of Types 304L and 316L SS, Incoloy 825, and Cu, but has virtually no effect on Cu–30%Ni and Cu–7%Al. The relative susceptibility of these materials to SCC determined from the preliminary SSRTs is being confirmed by additional SSRTs and also by tests on fracture–mechanics-type specimens.

ACKNOWLEDGMENTS

The authors thank W. E. Ruther for designing the water systems for the slow–strain–rate tests, W. K. Soppet for his help in the preparation and characterization of simulated J–13 water and W. F. Burke, D. E. Busch, S. L. Phillips, and F. E. Soppet for their contributions to various aspects of the experimental program.

REFERENCES

1. J. C. Farmer and R. D. McCright, "A Review of Models Relevant to the Prediction of Performance of High–Level Radioactive Waste Disposal Containers," CORROSION 89, Paper No. 519, National Association of Corrosion Engineers, Houston, Texas, 1989.

2. R. D. McCright, "FY 1985 Status Report on Feasibility Assessment of Copper–Base Waste Package Container Materials in a Tuff Repository,"

Lawrence Livermore National Laboratory-Report UCID-20509 DE86003960, Livermore, CA, September 1985.

3. A. E. Ogard and J. F. Kerrisk, "Groundwater Chemistry Along Flow Paths Between a Proposed Repository Site and the Accessible Environment," Los Alamos National Laboratory Report, LA-1088-MS, 1984.

4. P. S. Maiya, in "Environmentally Assisted Cracking in Light Water Reactors: Semiannual Report April-September 1986," NUREG/CR-4667, Vol. III ANL-87-37, Argonne National Laboratory Report, Argonne, IL September 1987.

5. P. S. Maiya, CORROSION J. (in press).

6. D. D. Macdonald, A. C. Scott, and P. Wentrcek, J. Electrochem. Soc., Vol. 126, No. 6, p. 908, 1979.

7. H. R. Copson, "Effect of Nickel Content on the Resistance to Stress-Corrosion Cracking of Iron-Nickel-Chromium Alloys in Chloride Environments" in First International Congress on Metallic Corrosion, Butterworths, London, p. 328, 1962.

8. W. Ramberg and W. R. Osgood, "Description of Stress-Strain Curves by Three Parameters," NACA Technical Note No. 902, July 1943.

9. H. Neuber, ASME J. Appl. Mech., Vol. 28, p. 544, 1961.

LIST OF TABLES

LIST OF FIGURES

Fig. 11. Effect of Strain Rate on SCC Susceptibility of Incoloy 925 in Simulated J–13 Water at 93°C.

Fig. 12. Effect of Strain Rate on SCC Susceptibility of Cu–30%Ni in Simulated J–13 Water at 93°C.

Table 1. Elemental Composition of Well J-13 Groundwater[a]

Element	Concentration (mg/L)	Anion	Concentration (mg/L)
Ca	11.5	F^-	2.1
Mg	1.76	Cl^-	6.4
Na	45.0	SO_4^{2-}	18.1
K	5.3	HCO_3^-	143.0
Li	0.06	NO_3^-	10.1
Fe	0.04		
Mn	0.001		
Al	0.03		
Si	30.0		

[a]Dissolved-oxygen concentration: 5.7 ppm; pH = 6.9.

Table 2. Chemical Composition (wt.%) of Austenitic Stainless Steels[a]

Element	304L SS (Heat V70200)	316L SS (Heat 16650)	Incoloy 825 (Heat HH2125F)
C	0.023	0.018	0.02
Mn	1.79	1.78	0.39
P	0.03	0.26	–
S	0.018	0.013	0.003
Si	0.39	0.43	0.14
Cr	18.15	16.5	21.98
Ni	8.25	10.39	43.89
Fe	Balance	Balance	27.98
Mo	0.3	2.09	2.79
Ti	–	–	0.75
Al	–	–	0.03
Cu	0.26	0.19	2.03
Co	0.14	0.10	–
N	0.079	0.054	–

[a]The chemical analyses were furnished by vendors. The vendors for Type 304L SS, Type 316L SS, and Incoloy 825 were Eastern Stainless Steel Co., Jessop Steel Co., and INCO Alloys International, respectively.

Table 3. Chemical Composition (wt.%) of Copper and Copper-Base Alloys[a]

Element	Copper[b] (Heat 7374)	Cu-30%Ni (Heat 673)	Cu-7%Al (Heat M5485)
Cu	99.90	69.52	90.69
Ni	–	29.4	–
Al	–	–	6.64
Pb	–	0.004	–
Fe	–	0.55	2.41
Zn	–	0.03	–
P	0.039	0.001	0.001
Mn	–	0.44	–
Cu	–	0.011	–
S	–	0.002	–

[a]The chemical analyses are furnished by vendors. The vendors for (phosphorus-deoxidized) copper, Cu-30%Ni, and Cu-7%Al are Revere Copper Products, Inc., Hussey Copper, Ltd., and Williams & Company, Inc., respectively.

Table 4. SSRT Results for Candidate Container Materials in Simulated J-13 Water at 93°C ($\dot{\varepsilon}$ = 1 x 10^{-7} s^{-1})

Test Number	Material	Heat Number	Specimen ECP, mV(SHE)	Elongation, ε_p (%)	Local Strain,[a] (%)	Nominal Stress Ratio[b]	Nominal Strain Ratio[c]
W1	IN 825	H2125F	233	4.9	15.1	0.93	0.82
W2	IN 825	H2125F	253	3.0	8.1	0.94	0.83
W3	Cu-30Ni	673	–	3.4	9.0	0.96	0.87
W4	304L	V70200	310	3.7	[d]	0.80	0.19
W5	Cu	7374	303	3.7	15.2	0.99	1.00
W6	316L	16650	268	3.6	[d]	0.81	0.51
W7	Cu-6Al	M5485	323	2.9	8.6	1.00	1.07
W12	Cu	7374	308	3.1	10.1	0.91	0.78

[a]The local strain is computed as the product of a strain concentration factor K_ε, estimated from Neuber's rule, and the nominal strain in the unreduced gage section, which is determined from the stress-strain curve and the measured load on the specimen. K_ε depends on the material and strain level.

[b]See Eq. (13).

[c]See Eq. (17).

[d]Too low to estimate accurately.

Table 5. SSRT Results for Candidate Container Materials in Simulated J-13 Water at 93°C ($\dot{\varepsilon}$ = 1 x 10^{-8} s^{-1})

Test Number	Material	Heat Number	Specimen ECP, mV(SHE)	Elongation, ε_p (%)	Local Strain[a] (%)	Nominal Stress Ratio[b]	Nominal Strain Ratio[c]
W13	IN 825	H2125F	383	1.2	[d]	0.87	0.40
W14	Cu-30Ni	673	293	1.3	2.3	0.97	0.88
W15	Cu-6Al	M5485	268	1.0	4.5	1.01	1.15
W18	Cu	7374	273	1.5	4.4	0.75	0.83
W19	316L	16650	374	1.6	[d]	0.72	0.15
W20	304L	V70200	343	1.6	[d]	0.52	-

[a]The local strain is computed as the product of a strain concentration factor K_ε, estimated from Neuber's rule, and the nominal strain in the unreduced gauge section, which is determined from the stress-strain curve and the measured load on the specimen. K_ε depends on the material and strain level.

[b]See Eq. (13).

[c]See Eq. (17).

[d]Too low to measure accurately.

Table 6. SEM Observations[a] on SSRT Specimens[b] of Candidate Waste Container Base Materials Tested in Simulated J-13 Water at 93°C.

Test No.	Material	Heat No.	Location	Cracking Observed
W1	Incoloy 825	H2125F	Top	yes
			Bottom	yes
W2	Incoloy 825	H2125F	Top	yes
			Bottom	yes
W3	Cu-30% Ni	673	Top	yes
			Bottom	yes
W4	304L SS	V70200	Top	yes
			Bottom	yes
W5	Cu	7374	Top	yes
			Bottom	yes
W6	316L SS	16650	Top	c
			Bottom	c
W7	Cu-6% Al	M5485	Top	yes
			Bottom	yes
W12	Cu	7374	Top	yes
			Bottom	yes

[a]All tests were conducted at a strain rate of 10^{-7} s^{-1} and interrupted after nominal strains of 3-4%. SEM observations were made at magnifications between 100X and 2000X.

[b]The specimen has two holes with pins of the same material inserted into them to produce tight crevices. The specimen was exposed to J-13 water in such a way that the top hole with the pin was alternately exposed to water in liquid and vapor phases, but the bottom hole was always immersed in J-13 water.

[c]This specimen was pulled to failure in liquid nitrogen following the interrupted test to determine the feasibility of determining the crack length, but it was not possible to examine the extent of cracking on the fracture surface.

Table 7. Yield Stress of Candidate Waste Container Materials.[a]

Material	Heat Number	Yield Stress, Ksi (MPa)
304L SS	V70200	40.5 (279)
316L SS	16650	37.3 (257)
Incoloy 825	H2125F	50.5 (348)
Cu	7374	11.4 (79)
Cu–7%Al	M5485	44.6 (307)
Cu–30%Ni	673	23.8 (164)

[a]Tensile tests on smooth specimens were performed in air at room temperature at a strain rate of $2.2 \times 10^{-4}\ s^{-1}$.

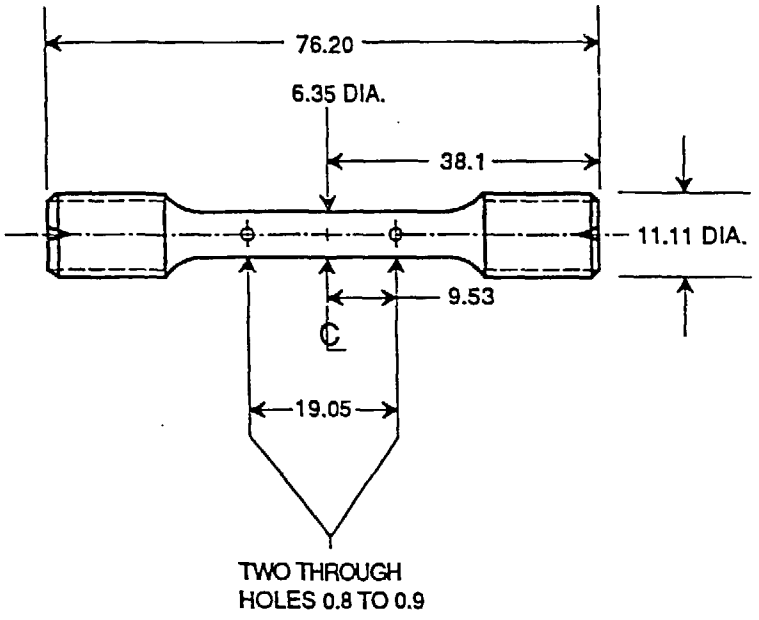

Fig. 1. Fabrication Drawing for SSRT Specimen. Dimensions are in mm.

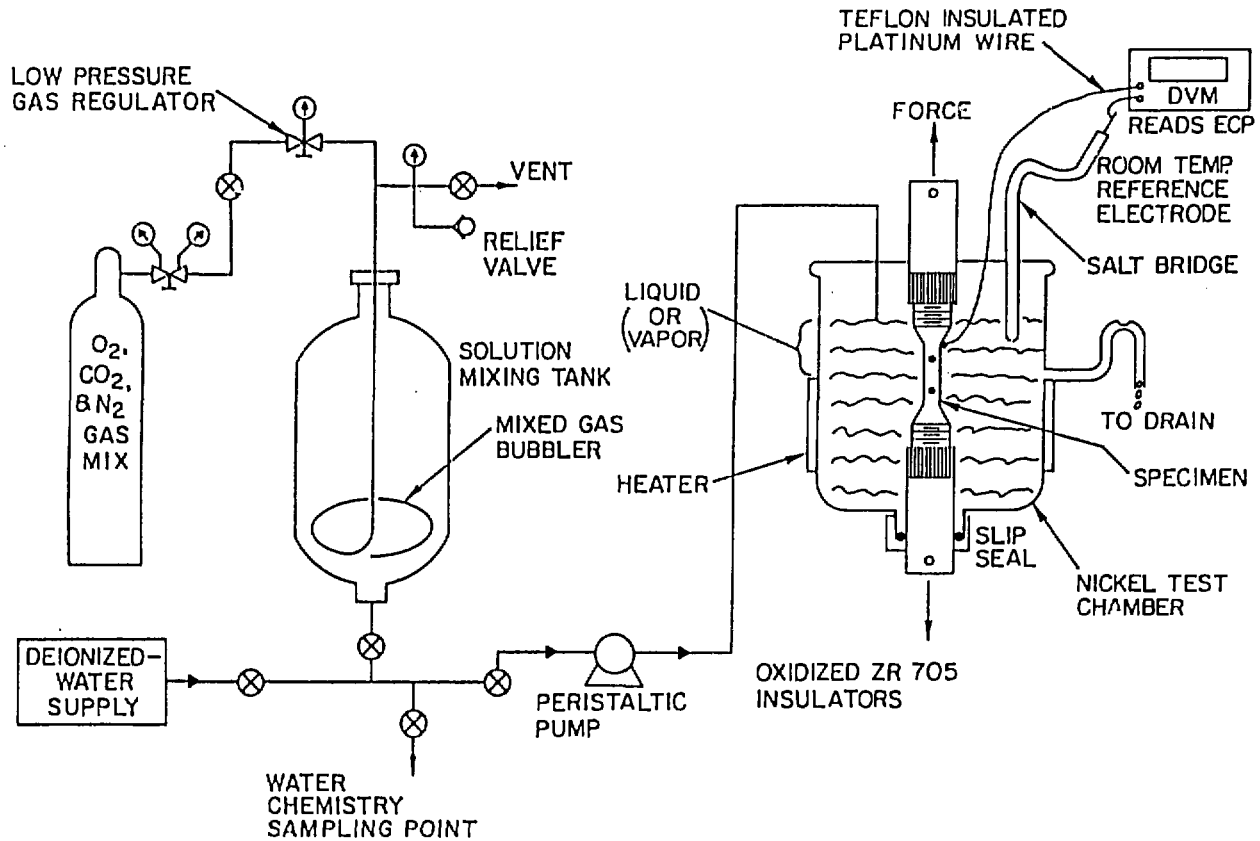

Fig. 2. Schematic Representation of the SSRT Setup with Feedwater an Electro-Chemical-Potential Monitoring Systems.

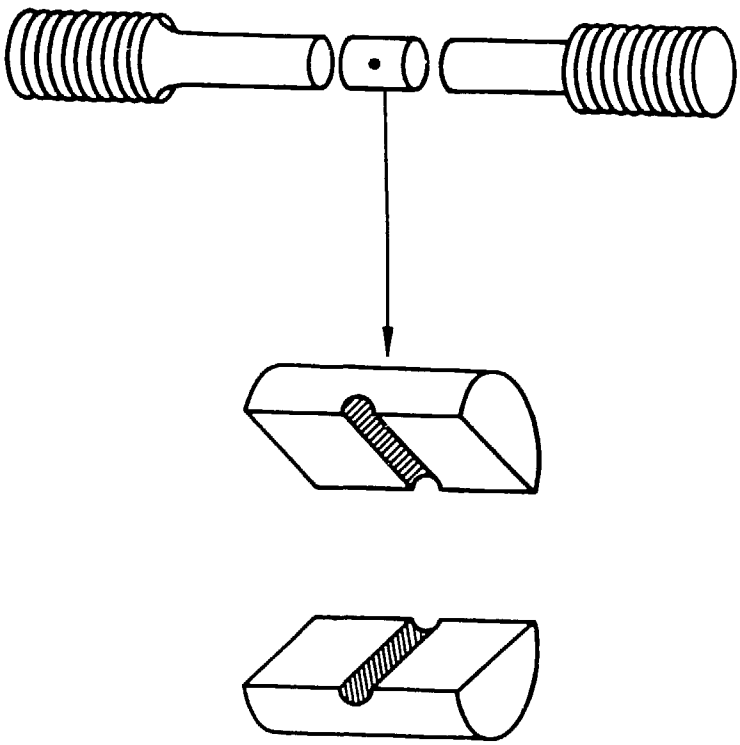

Fig. 3. Cross-Sectional View of Drilled Hole in SSRT Specimen.

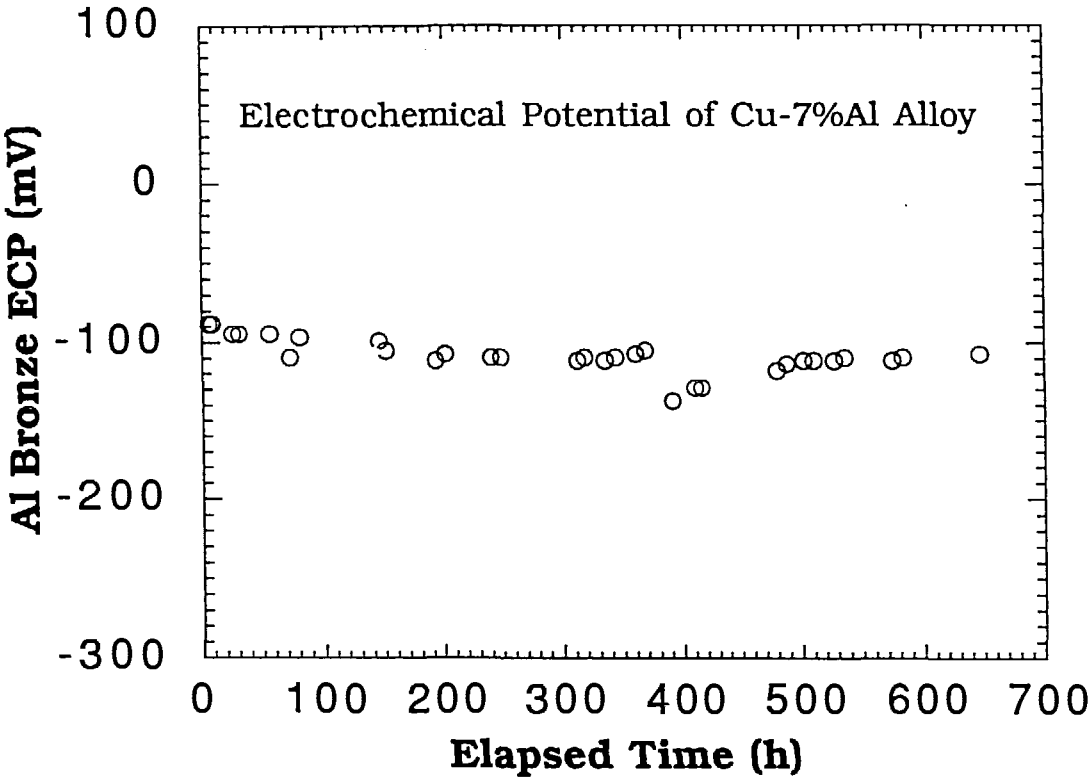

Fig. 4. Electrochemical Potential of Cu–7%Al Alloy Specimen at 93°C against an External 2 x 10^{-4} M KCl/Ag/AgCl Reference Electrode as a Function of Time during Test W15.

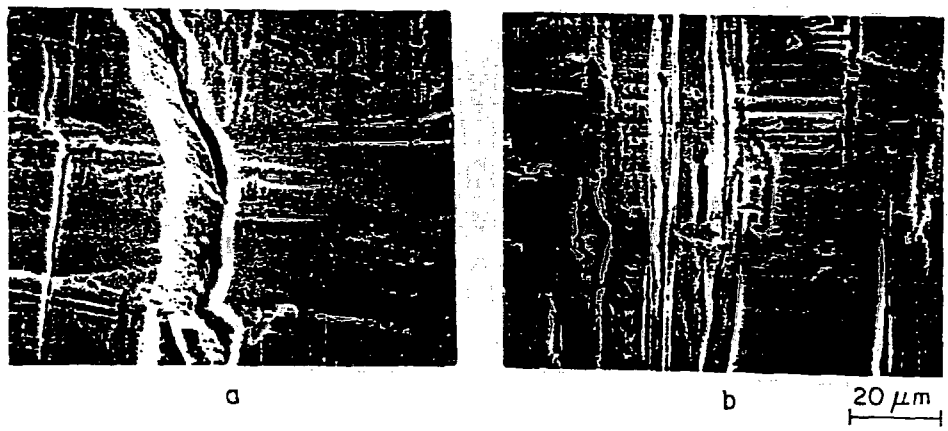

Fig. 5. SEM Photomicrographs of Hole Regions (with Pins) of (a) Type 304L SS, Interrupted after ε_p = 3.7%, and (b) Incoloy 825 Interrupted after ε_p = 3.0% ($\dot{\varepsilon}$ = 1 x 10^{-7} s^{-1}).

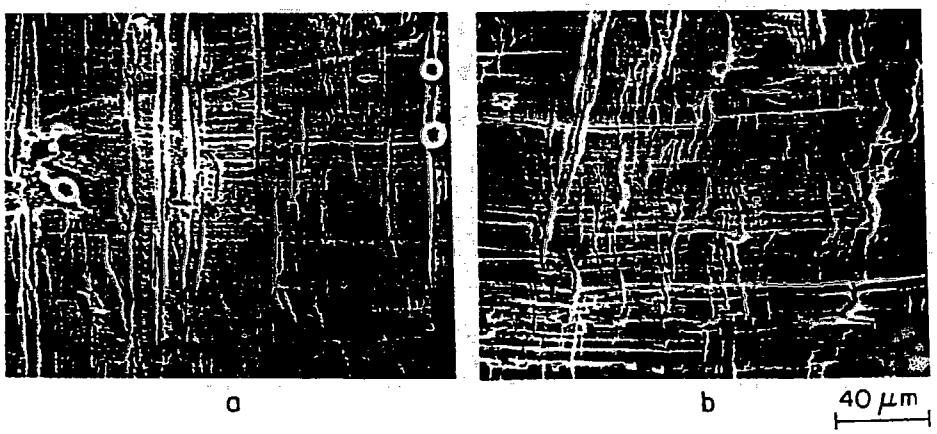

Fig. 6. SEM Photomicrographs of Hole Regions of Incoloy 825 Interrupted after ε_p = 3.0%: (a) Exposed to Liquid, and (b) Exposed to Alternating Liquid and Vapor ($\dot{\varepsilon} = 1 \times 10^{-7}\ s^{-1}$).

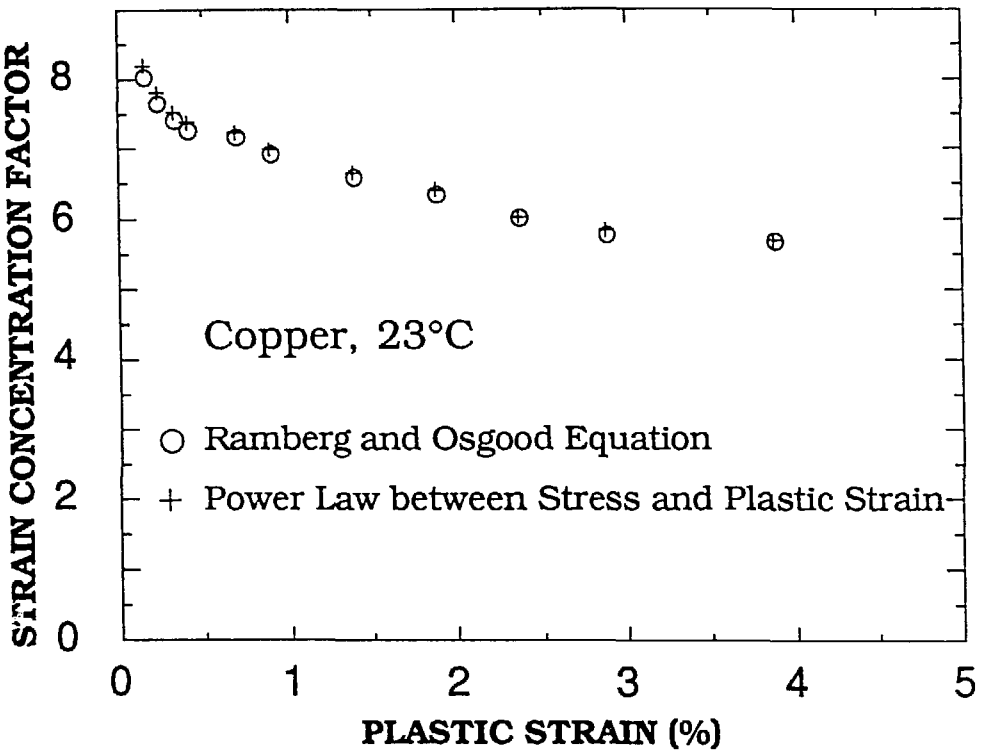

Fig. 7. Strain Concentration Factor as a Function of Plastic Strain for Cu.

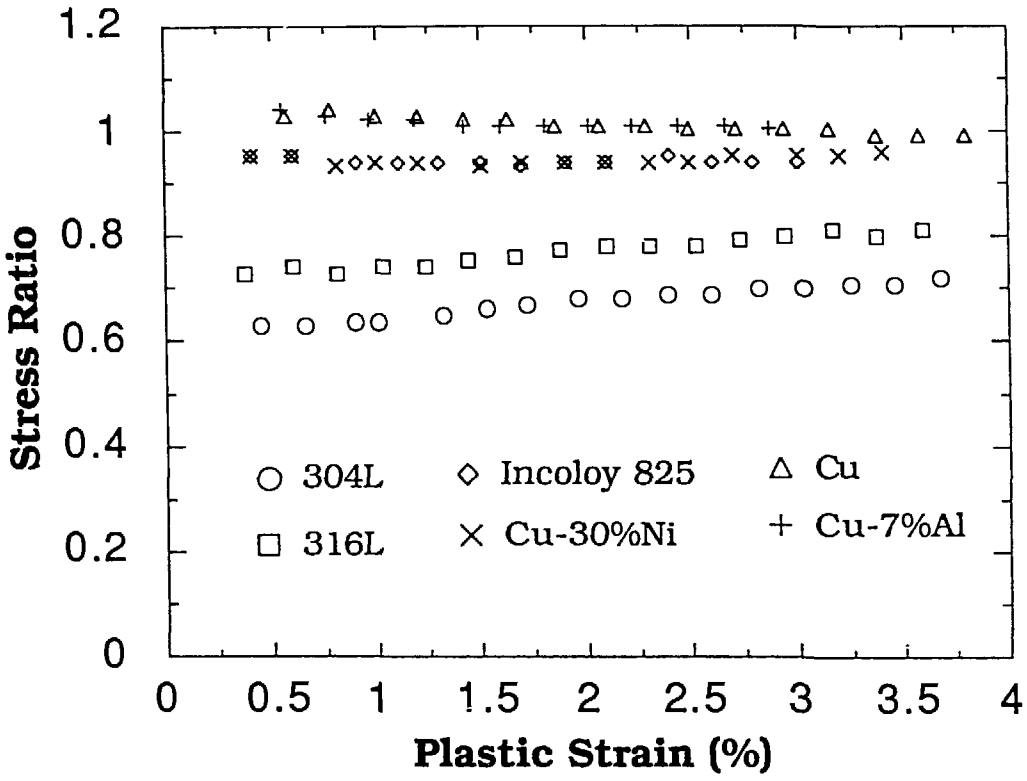

Fig. 8. Relative Cracking Susceptibility of Six Candidate Materials in Simulated Well J-13 Water at 93°C. Cracking Susceptibility is expressed in terms of the nominal stress ratio (defined in text) where lower values imply greater cracking susceptibility ($\dot{\varepsilon} = 1 \times 10^{-7}\ s^{-1}$).

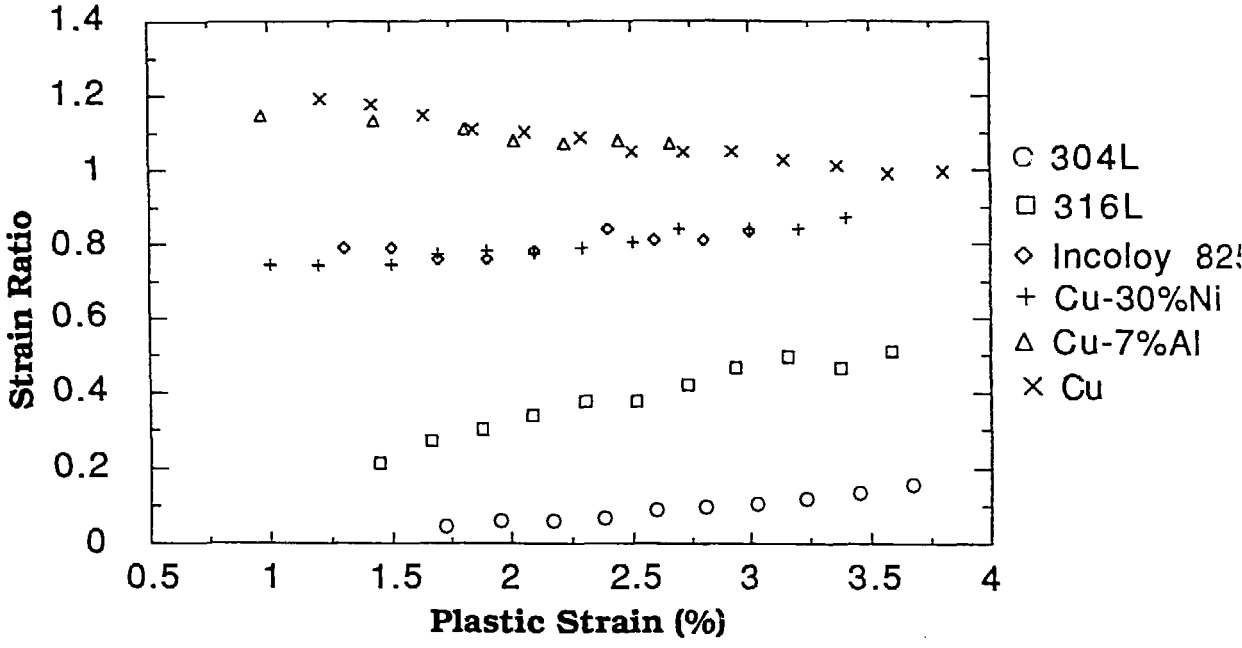

Fig. 9. Relative Cracking Susceptibility of Six Candidate Materials in Simulated J-13 Water at 93°C. Cracking susceptibility is expressed in terms of nominal strain ratio where lower values imply greater cracking susceptibility
($\dot{\varepsilon}$ =1 x 10^{-7} s^{-1}).

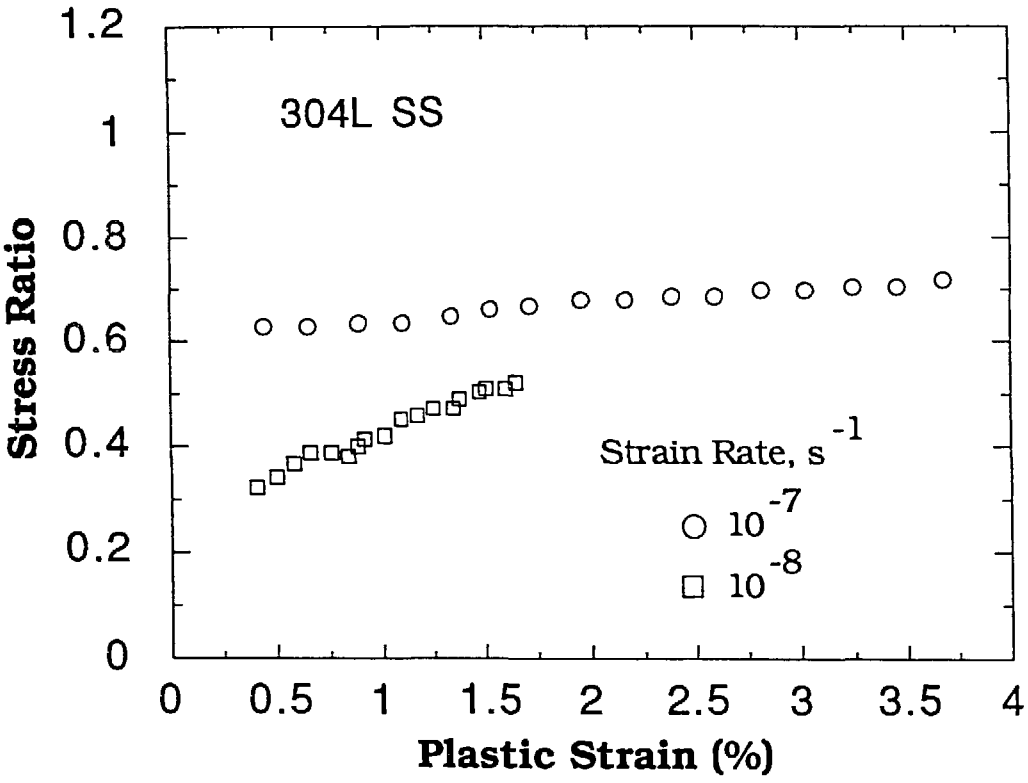

Fig. 10. Effect of Strain Rate on SCC Susceptibility of Type 304L SS in Simulated J-13 Water at 93°C.

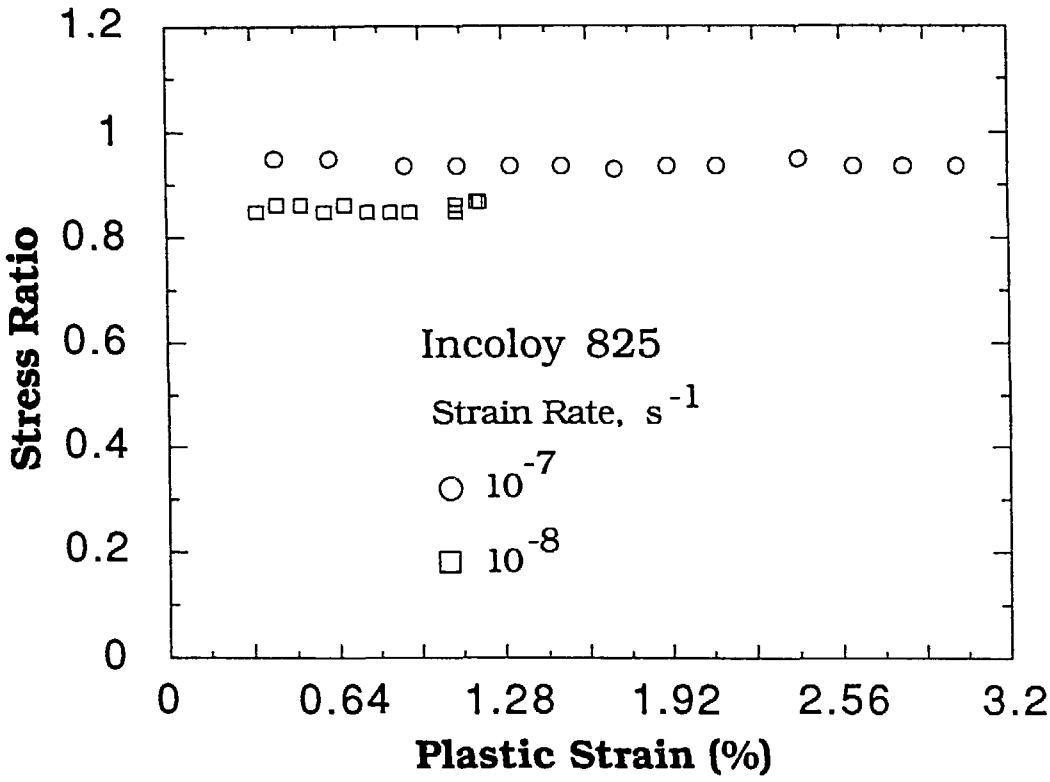

Fig. 11. Effect of Strain Rate on SCC Susceptibility of Incoloy 825 in Simulated J-13 Water at 93°C.

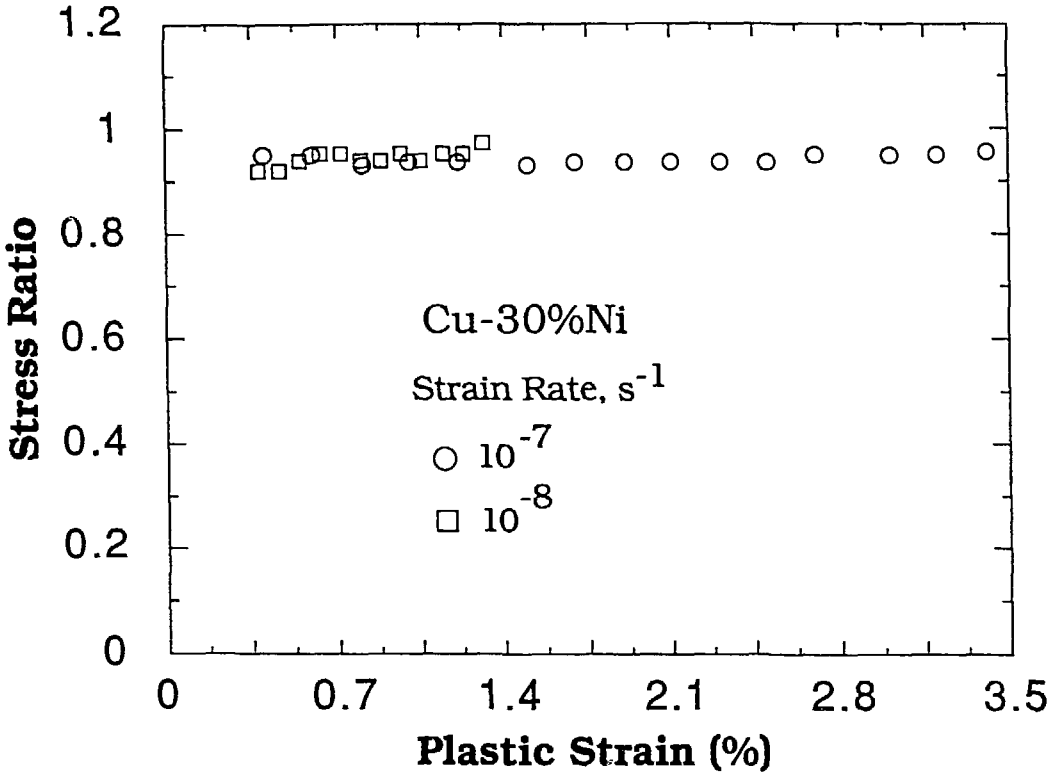

Fig. 12. Effect of Strain Rate on SCC Susceptibility of Cu-30%Ni in Simulated J-13 Water at 93°C.